Activation of Dihydrogen and Si lanes by Cationic Iron Bis(phosphinite) Pincer Complexes

ARTICLE *in* ORGANOMETALLICS · NOVEMBER 2014

Impact Factor: 4.13 · DOI: 10.1021/om500758j

ORGANOMETALLICS

Article

pubs.acs.org/Organometallics

Activation of Dihydrogen and Silanes by Cationic Iron Bis(phosphinite) Pincer Complexes

Papri Bhattacharya, Jeanette A. Krause, and Hairong Guan*

Department of Chemistry, University of Cincinnati, P.O. Box 210172, Cincinnati, Ohio 45221-0172, United States

Supporting Information

ABSTRACT: Treatment of iron POCOP-pincer hydride complexes *cis*-[2,6-(^{i}Pr$_2$PO)$_2$C$_6$H$_3$]Fe(H)(PMe$_3$)$_2$ (**1-H**), [2,6-(^{i}Pr$_2$PO)$_2$C$_6$H$_3$]-Fe(H)(PMe$_3$)(CO) (**2-H**, *trans* H/CO; **2′-H**, *cis* H/CO), and *cis*-[2,6-(^{i}Pr$_2$PO)$_2$C$_6$H$_3$]Fe(H)(CO)$_2$ (**3-H**) with HBF$_4$·Et$_2$O in CD$_3$CN/THF-d_8 results in a rapid evolution of H$_2$. Except for the reaction of **1-H**, which leads to decomposition of the pincer structure, all other hydrides are converted cleanly to acetonitrile-trapped cationic complexes. Protonation of these hydrides with the weaker acids CF$_3$CO$_2$H and HCO$_2$H establishes the basicity order of **1-H** > **2-H** > **2′-H** > **3-H**, with **3-H** bearing the least basic hydride ligand. An alternative method of abstracting hydride by [Ph$_3$C]$^+$[BF$_4$]$^-$ gives complicated products; the reaction of **2-H** generates two pincer products, [HPMe$_3$]$^+$[BF$_4$]$^-$ and Gomberg's dimer, which supports a single electron transfer pathway. Cationic complexes {[2,6-(^{i}Pr$_2$PO)$_2$C$_6$H$_3$]Fe(CO)(PMe$_3$)(CH$_3$CN)}$^+$[BF$_4$]$^-$ (**2$^+$-BF$_4$**, *trans* CO/CH$_3$CN) and *cis*-{[2,6-(^{i}Pr$_2$PO)$_2$C$_6$H$_3$]Fe(CO)$_2$(CH$_3$CN)}$^+$[BF$_4$]$^-$ (**3$^+$-BF$_4$**) are prepared from protonation of **2-H** (or **2′-H**) and **3-H** with HBF$_4$·Et$_2$O, respectively. Both compounds react with H$_2$ with the aid of ^{i}Pr$_2$NEt to yield neutral hydride complexes and [^{i}Pr$_2$N(H)Et]$^+$[BF$_4$]$^-$. In addition, they catalyze the hydrosilylation of benzaldehyde and acetophenone with (EtO)$_3$SiH and show higher catalytic activity than the neutral hydrides **2-H**/**2′-H** and **3-H**. The mechanism for the formation of **2$^+$-BF$_4$** and the X-ray structure of **2$^+$-BF$_4$** are also described.

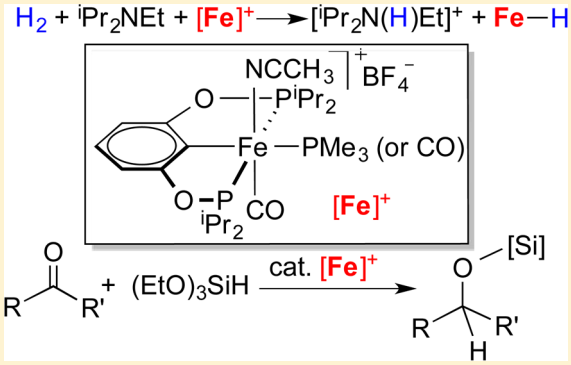

INTRODUCTION

Transition metal catalyzed reduction of polar bonds is an essential process in fine or commodity chemical synthesis.[1] The efficiency of a catalytic system is sometimes directly linked to how effectively the metal can activate the reducing agents (e.g., H$_2$, silanes, and boranes). Among various activation strategies,[2−4] the use of cationic complexes has resulted in tremendous success for a myriad of reduction processes,[5] particularly hydrosilylation reactions.[6−11] A generalized (and simplified) mechanism that features a cationic catalyst is illustrated in Scheme 1 using a ketone as a representative substrate. When cationic and coordinatively unsaturated, the metal center often has a good binding affinity for H−E (E = H, SiR$_3$), resulting in a σ-complex and/or the oxidative addition product. Forming the latter is usually less favorable for a cationic species due to little back-donation from an electrophilic metal to the H−E σ* orbital. Nevertheless, the subsequent stepwise, outer-sphere transfer of E$^+$ and H$^-$ to the ketone substrate completes the catalytic cycle.

Hydrogenation reactions following this mechanism are best known as ionic hydrogenation, which has been thoroughly reviewed by Bullock.[12] In terms of reduction with silanes, cationic iridium bis(phosphinite) pincer (also known as POCOP-pincer) complexes have shown remarkable activity for catalytic hydrosilylation of compounds bearing C−O or C═O bonds.[10] Mechanistic studies have supported catalytic

Scheme 1. Catalytic Reduction of a Ketone with a Cationic Complex

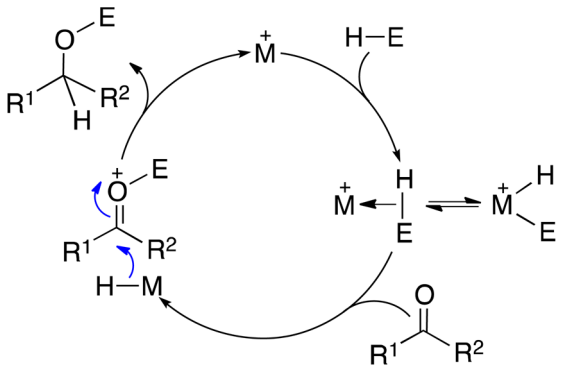

cycles with general features of Scheme 1.[13,14] This type of mechanism has also been proposed for hydrosilylation reactions catalyzed by [CpW(CO)$_2$(IMes)]$^+$[B(C$_6$F$_5$)$_4$]$^-$,[6a] cationic Re(V) oxo complexes,[7] and [CpRu(^{i}Pr$_3$)(CH$_3$CN)$_2$]$^+$.[9b,c,e]

We have reported that iron hydride complexes with a POCOP-pincer ligand (Figure 1) are effective catalysts for the hydrosilylation of aldehydes/ketones[15] and the dehydrogenation of

Received: July 28, 2014
Published: October 16, 2014

   dx.doi.org/10.1021/om500758j | *Organometallics* 2014, 33, 6113−6121

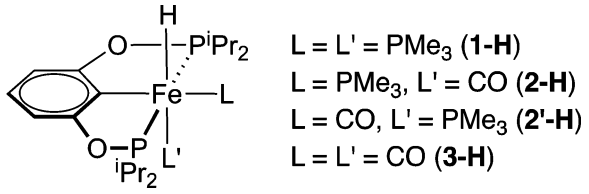

Figure 1. Iron hydride complexes with a POCOP-pincer ligand.

ammonia borane.[16] Our mechanistic analyses have suggested that the hydride ligand remains intact during catalysis, but helps facilitate the dissociation of the *trans* ligand L′ for substrate binding. Wei and co-workers have recently studied our hydrosilylation system computationally.[17] Their DFT calculations have pointed out that the pathway with the lowest kinetic barrier begins with ligand substitution by a carbonyl substrate followed by C═O insertion into the Fe−H bond. Such a mechanism is, however, inconsistent with our observation that the reaction of PhCDO, Ph_2SiD_2, and **1-H** generates $Ph_2SiD(OCD_2Ph)$ and $Ph_2Si(OCD_2Ph)_2$ with no deuterium incorporated into **1-H**.

In this work, we remove the hydride ligand of these iron pincer complexes via protonation reactions. The resulting cationic compounds are still active catalysts for the hydrosilylation of benzaldehyde and acetophenone. In fact, they are more reactive than the parent neutral hydride complexes. We also describe stoichiometric activation of H_2 by the cationic pincer complexes in the presence of an externally added base.

RESULTS AND DISCUSSION

Abstraction of the Hydride Ligand. Our initial strategy to remove the hydride ligand from iron was to treat the complexes in Figure 1 with $[Ph_3C]^+[BF_4]^-$. Mixing **1-H** with $[Ph_3C]^+[BF_4]^-$ in CD_2Cl_2 led to the rapid disappearance of the hydride species as confirmed by ^{1}H NMR; however, the $^{31}P\{^1H\}$ NMR spectrum displayed two resonances, one at 40.5 ppm (major) and the other at −13.0 ppm (minor). These chemical shifts are indicative of a breakdown of the pincer framework.[18] The reaction of **2-H** with $[Ph_3C]^+[BF_4]^-$ in CD_2Cl_2 resulted in a complicated mixture featuring very broad ^{1}H NMR resonances. Fortunately, the same reaction carried out in a coordinating solvent, CD_3CN, was much more informative due to well-resolved NMR peaks. The spectra recorded at 1 h revealed three pincer complexes: the unreacted **2-H**, acetonitrile-trapped complex $\mathbf{2}^+$-$\mathbf{BF_4}$ (*vide infra*), and the third iron complex assigned as bis(acetonitrile) complex $\mathbf{4}^+$-$\mathbf{BF_4}$ (eq 1).

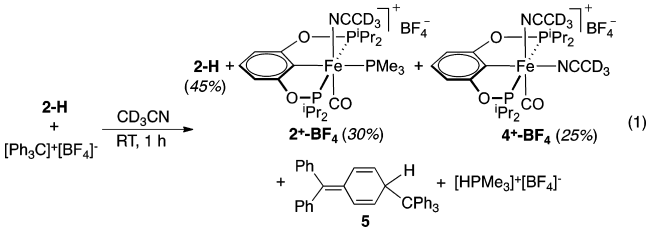

(1)

The mass spectrum of the reaction mixture showed ions $\mathbf{2}^+$ (m/z 542) and $\mathbf{4}^+$ (m/z 507) as well as their expected fragmentations. $\mathbf{4}^+$-$\mathbf{BF_4}$ was assigned as a *cis*-bis(acetonitrile) complex based on the observation of two sets of methine resonances; the more symmetric *trans* isomer should have one set of methine resonances. The ^{1}H NMR spectrum also showed the formation of Gomberg's dimer **5**[19] and $[HPMe_3]^+[BF_4]^-$.

The presence of **5** is a strong indication of single electron transfer (SET) from **2-H** to $[Ph_3C]^+[BF_4]^-$, resulting in $[\mathbf{2\text{-}H}]^{+\bullet}$ and the trityl radical (which dimerizes to give **5**). Radical cations of this type are known to be acidic enough to protonate their original hydride complexes[20] and in this case PMe_3 as well.

To avoid the complications associated with SET, we resorted to Brønsted acids to remove the hydride ligand.[21] The success of such a process is obviously dependent on the strength of the acid used. Table 1 summarizes the protonation results using

Table 1. Extent of Protonation of Iron Hydrides by Different Acids[a]

entry	acid	1-H	2-H	2′-H	3-H
1	$HBF_4{\cdot}Et_2O$	>99%[b]	>99%	>99%	>99%
2	CF_3CO_2H	>99%[b]	>99%	34%	0%[c]
3	HCO_2H	31%[b]	5%	0%[c]	0%[c]

[a]Conditions: hydride (10 μmol) and acid (10 μmol) mixed in CD_3CN/THF-d_8 (1:1, ∼0.5 mL total) at −30 °C and then warmed to RT (for $HBF_4{\cdot}Et_2O$) or at RT (for CF_3CO_2H and HCO_2H) until the equilibrium was reached. [b]Decomposition of the pincer complex was observed. [c]Reaction was monitored for 48 h.

acids with varying pK_a values, which provide a qualitative sense of the basicity of the iron hydride complexes. The protonation reactions were carried out in CD_3CN/THF-d_8 (1:1) and monitored by NMR spectroscopy. The role of CD_3CN was to intercept any coordinatively unsaturated species prior to decomposition, and THF-d_8 was added to improve solubility. Reactions of the iron hydrides with 1 equiv of $HBF_4{\cdot}Et_2O$ (pK_a = 0.1 in CH_3CN[22,23]) were fast at −30 °C, resulting in a rapid loss of H_2. Within a few minutes, the color of the solutions turned to bright yellow. The change in color was more vivid in the cases of **2-H**, **2′-H**, and **3-H**, as they are either pale yellow (**2-H**) or almost colorless (**2′-H** and **3-H**). The ^{1}H NMR spectra confirmed the disappearance of the hydride resonance but with no evidence for a dihydrogen or dihydride species. Unlike the other hydride complexes, the reaction of **1-H** led to extensive decomposition and the formation of $HPMe_3^+$. Evidently, $HBF_4{\cdot}Et_2O$ protonates not only the hydride ligand but also PMe_3; hence it causes the collapse of the pincer scaffold. While all the hydrides described in this study are fully protonated by $HBF_4{\cdot}Et_2O$ (entry 1), using weaker acids differentiates the basicity of these complexes. When CF_3CO_2H (pK_a = 12.7 in CH_3CN[22,23]) was added to the solution of **1-H** or **2-H** at room temperature, the hydride resonance disappeared within a few minutes (entry 2). On the other hand, only 34% of **2′-H** was protonated under similar conditions, and no protonation reaction was observed for **3-H**. Using an even weaker acid (HCO_2H)[24] resulted in 31% of **1-H** being protonated (entry 3). Analogous to the reactions with $HBF_4{\cdot}Et_2O$ and CF_3CO_2H, substantial decomposition was observed in this case. Treatment of **2-H** with HCO_2H converted merely 5% of **2-H**, while **2′-H** and **3-H** did not undergo protonation at all.

The aforementioned protonation data suggest that the relative basicity of the iron hydride complexes follows a decreasing order of **1-H** > **2-H** > **2′-H** > **3-H**. The kinetic site for the protonation should be the hydride ligand, as demonstrated in related systems.[25] However, no dihydrogen complexes were observed, suggesting that the dihydrogen molecule is weakly bound to iron and readily displaced by CD_3CN. The relative basicity of the iron hydride complexes is consistent with the order of electron density at the iron center.

dx.doi.org/10.1021/om500758j | *Organometallics* 2014, 33, 6113−6121

A more electron-rich iron center is likely to induce more negative charge on the hydride ligand, thus making the protonation more readily. The presence of the electron-donating PMe_3 ligand makes the Fe−H more basic; thus the bis-PMe_3 complex **1-H** is most readily protonated. As the PMe_3 ligand is substituted by a π-accepting CO ligand, the electron density at the metal is reduced and the basicity decreases. Complexes **2-H** and **2′-H** have identical supporting ligands, but **2-H** is more basic than **2′-H**, likely due to its hydride being disposed at the opposite side of the stronger *trans*-influencing ligand CO.

Synthesis of Cationic Iron Pincer Complexes. Because $HBF_4{\cdot}Et_2O$ readily protonates all the iron hydrides, it was chosen as the acid to synthesize the targeted cationic pincer complexes. In the presence of CH_3CN as a coordinating solvent, the reactions of **2-H** (eq 2) and **3-H** (eq 3) with $HBF_4{\cdot}$

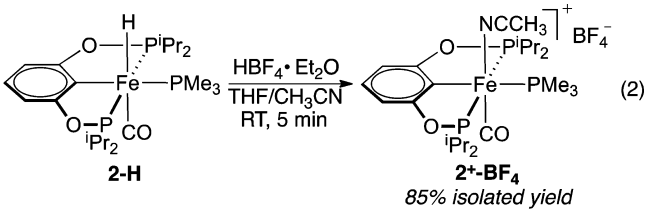

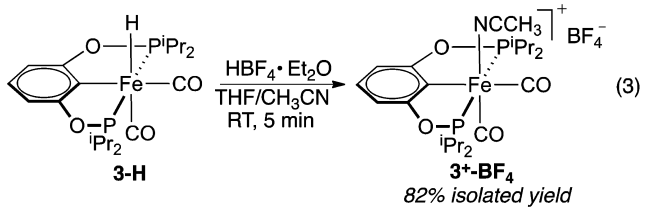

Et_2O led to CH_3CN-trapped complexes **2**$^+$-BF_4 and **3**$^+$-BF_4, respectively. The $^{31}P\{^1H\}$ spectrum of **2**$^+$-BF_4 reveals a triplet at −0.2 ppm for PMe_3 and a doublet at 206.4 ppm for the phosphinite ligand. The magnitude of the $^{31}P-^{31}P$ coupling constant for **2**$^+$-BF_4 (16.5 Hz) is comparable to that for **2-H** (14.9 Hz), implying that these two complexes have the same spatial arrangement for PMe_3 and the pincer ligand. For comparison, **2′-H**, in which PMe_3 and the *ipso* carbon are *cis* to each other, gives a much larger $^{31}P-^{31}P$ coupling constant of 29.6 Hz. In the case of **3**$^+$-BF_4, two ^{13}C resonances (205.5 and 210.5 ppm) appear in the region for a carbonyl group, which is consistent with a C_s symmetry structure bearing two *cis* CO ligands. As expected, ^1H NMR of **3**$^+$-BF_4 shows two sets of multiplets for the methine hydrogens of the isopropyl groups.

The structure of **2**$^+$-BF_4 was more unambiguously established by X-ray crystallography. As shown in Figure 2, CH_3CN is located *trans* to the carbonyl group and the PMe_3 ligand remains *trans* to the *ipso* carbon. Structural comparison between **2**$^+$-BF_4 and **2-H** (Table 2) reveals some noticeable differences in bond lengths and angles. Compared to **2-H**, all the Fe−P bonds of **2**$^+$-BF_4 are elongated by 0.06−0.10 Å. Although the Fe−C_{ipso} distance is almost identical, the Fe−C22 bond is shortened by 0.04 Å, reflecting a decreasing *trans* influence changing from H^- to CH_3CN. Interestingly, **2**$^+$-BF_4 has a wider P1−Fe−P2 angle than **2-H** [156.83(2) vs 149.81(3) Å], which is mainly due to how the pincer ligand distorts from a perfect meridional geometry. The chelating rings of POCOP-pincer systems bearing an aromatic backbone are flat in general,[26] but the iron pincer complexes are substantially less planar for the core structure, perhaps due to a more crowded octahedral geometry about iron.[27] In **2**$^+$-BF_4, the pincer ligand adopts an asymmetric bend conformation (Figure 3) with the phosphorus atoms being displaced +0.4950 and −0.2988 Å out of the least-squares plane defined by the C1, O1, O2, and Fe.[28] In contrast, **2-H** has a "gull wing"

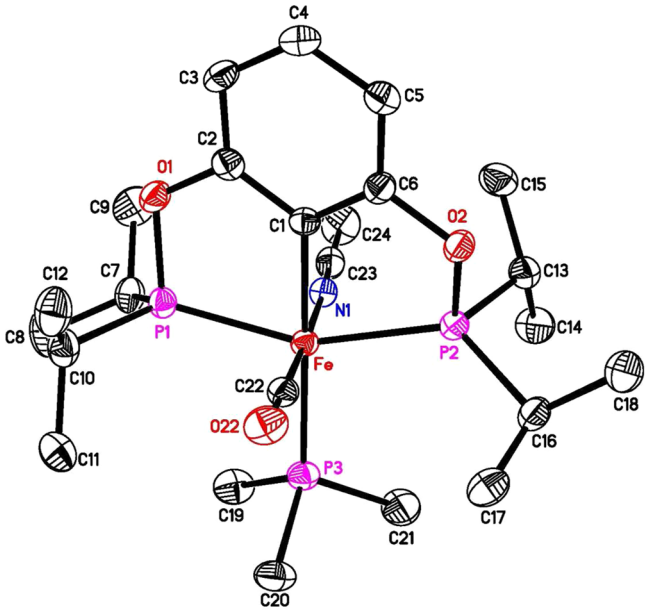

Figure 2. ORTEP drawing of {[2,6-(^{i}Pr$_2$PO)$_2$C$_6$H$_3$]Fe(CO)(PMe$_3$)-(CH$_3$CN)}$^+$[BF$_4$]$^-$ (**2**$^+$-BF_4) at the 50% probability level. For clarity, the counterion BF_4^- is not shown.

Table 2. Selected Bond Lengths (Å) and Angles (deg) for Complexes 2$^+$-BF_4 and 2-H

	2$^+$-BF_4	**2-H**[a]
Fe−C(1)	2.001(2)	2.013(2)
Fe−P(1)	2.2594(7)	2.2002(6)
Fe−P(2)	2.2854(7)	2.1888(7)
Fe−P(3)	2.2888(7)	2.2198(6)
Fe−C(22)	1.731(2)	1.774(2)
C(22)−O(22)	1.155(3)	1.157(3)
C(1)−Fe−P(1)	79.23(6)	79.43(7)
C(1)−Fe−P(2)	78.06(6)	77.58(7)
C(1)−Fe−P(3)	177.86(6)	176.78(6)
P(1)−Fe−P(2)	156.83(2)	149.81(3)
P(2)−Fe−P(3)	102.18(3)	102.04(2)
P(1)−Fe−P(3)	100.68(3)	99.81(2)
C(2)−O(1)−P(1)	113.75(13)	113.08(13)
C(6)−O(2)−P(2)	112.48(13)	110.23(14)

[a]The crystal structure of **2-H** was reported earlier by us (see ref 15).

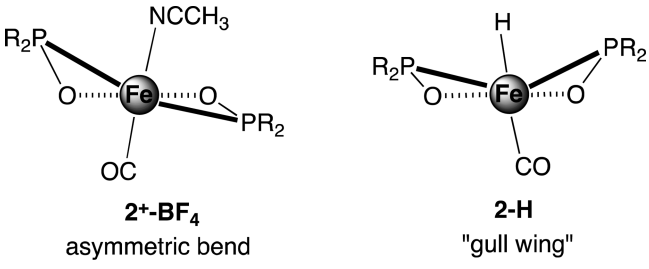

Figure 3. Distortion of the pincer ligand in **2**$^+$-BF_4 and **2-H**.

dx.doi.org/10.1021/om500758j | *Organometallics* 2014, 33, 6113−6121

Scheme 2. Protonation of 2-H and 2′-H Involving Square-Pyramidal Intermediates

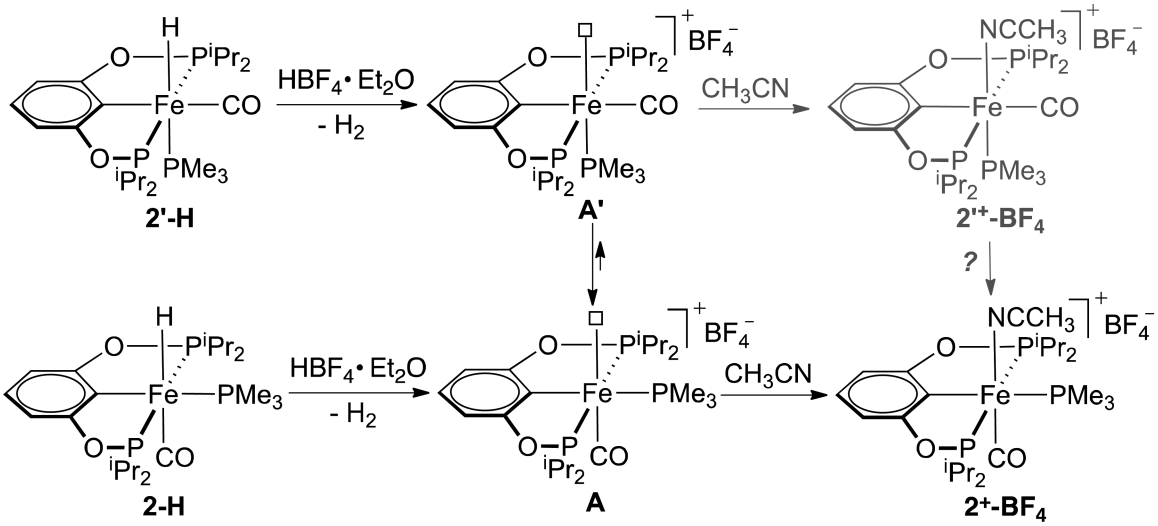

Scheme 3. Protonation of 2-H and 2′-H Involving a Distorted Trigonal-Bipyramidal Intermediate

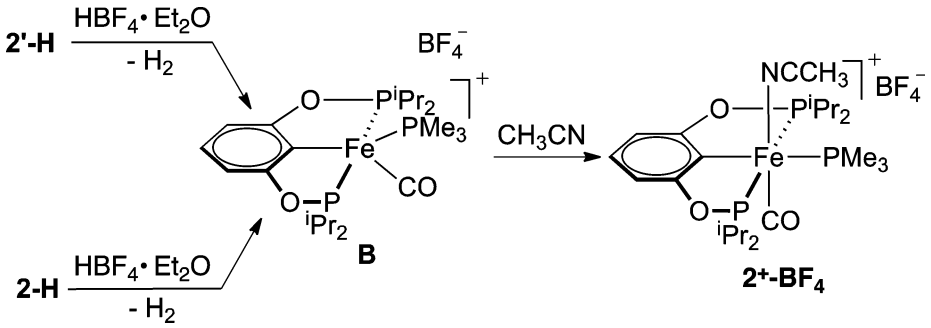

conformation[26] to take advantage of the small size of the hydride ligand, resulting in the phosphorus atoms deviating from the C1−O1−O2−Fe plane by +0.5135 and +0.2161 Å.[29]

Although **1-H** reacts with $HBF_4{\cdot}Et_2O$, attempts to isolate the corresponding cationic complex failed even when the protonation reaction was carried out at low temperatures. Switching the acid to CF_3COOH did not improve the synthesis. The purification was hampered by the formation of $HPMe_3^+$, free diphosphinite ligand, and other decomposition products.

The reaction of **2′-H** with $HBF_4{\cdot}Et_2O$, on the other hand, cleanly afforded one pincer-ligated complex, which was obtained in 84% yield after workup. The ^1H, $^{13}C\{^1H\}$, and $^{31}P\{^1H\}$ NMR and IR data and crystal structure determination of the isolated compound match well with those of **2**$^+$**-BF**$_4$, suggesting that PMe_3 and CO swap their positions during the reaction. A mechanism consistent with this result is outlined in Scheme 2. Upon protonation of the hydride and loss of H_2, the square-pyramidal intermediate **A**′ would rapidly isomerize to **A** so that the two strongly *trans*-influencing ligands (CO and aryl group) avoid being *trans* to each other. Trapping of the predominant intermediate **A** with CH_3CN produces **2**$^+$**-BF**$_4$. A similar mechanism has been proposed by Kirchner for the carbonylation of $Fe(PNP)(X)_2(CO)$ (PNP = aminophosphine-based pincer ligands[30]) facilitated by $AgBF_4$.[31] In that study, regardless of which geometric isomer (*cis* or *trans*) was used, abstraction of halide from $Fe(PNP)(X)_2(CO)$ provided the same 16-electron intermediate, $[Fe(PNP)(X)(CO)]^+$, which is analogous to **A** with CO occupying the apical position of the square pyramid. Trapping of $[Fe(PNP)(X)(CO)]^+$ by CO gave *trans*-$[Fe(PNP)(X)(CO)_2]^+$ exclusively.

Although we cannot rule out the possibility of isomerization of a kinetically trapped product **2**′$^+$**-BF**$_4$ to **2**$^+$**-BF**$_4$ (shaded in gray in Scheme 2), such a mechanism seems less likely. We have previously shown that geometric isomerization of 18-electron iron POCOP-pincer complexes places CO *trans* to the pincer aromatic ring.[15] Similar observations have been made by others in *cis*-to-*trans* isomerization of $(PCP)Ir(H)_2CO$[32] and $(PNP)Fe(X)_2CO$.[33] DFT calculations carried out by Hall on the iridium system have suggested that the isomerization process is driven by a delocalized interaction between the π orbitals of CO, the d_π orbital of Ir, and the π orbitals of the pincer aromatic ring in the *trans* isomer.[34] Therefore, we had anticipated that **2**′$^+$**-BF**$_4$ would be thermodynamically more stable than **2**$^+$**-BF**$_4$.

Protonation of **2-H** and **2′-H** could converge to a Y-shaped, distorted trigonal-bipyramidal intermediate **B** (Scheme 3), and the subsequent coordination of CH_3CN to the iron center of **B** might selectively give **2**$^+$**-BF**$_4$. This mechanism is also disfavored because the Y-structure generally requires the ligand *trans* to the acute angle (in this case, the angle formed by CO and PMe_3) to be a weak σ-donor and a good π-donor.[35] Ligands that fit this criterion are usually halides, amides, and alkoxides. Although **B** is less likely to be a ground-state structure, it could be the transition state for the interconversion between **A** and **A**′.

Activation of Dihydrogen. Protonation of the neutral iron pincer hydrides to yield the cationic complexes is, in principle,

dx.doi.org/10.1021/om500758j | *Organometallics* 2014, 33, 6113−6121

a reversible process. Having a base with an appropriate pK_b value, the cationic dihydrogen intermediate can be reverted back to the neutral hydride, thereby activating H_2 in a heterolytic (H^+/H^-) fashion. The protonation results shown in Table 1 imply that the pK_a value for the conjugate acid of **2-H** should fall in between the values for CF_3CO_2H and HCO_2H, and therefore a typical amine should be able to assist with H_2 activation. Indeed when a mixture of **2**$^+$-**BF**$_4$ and ^{i}Pr$_2$NEt (Hünig's base) in CH_2Cl_2 was exposed to H_2, the color of the solution changed from yellow to almost colorless, suggesting the consumption of **2**$^+$-**BF**$_4$. Within 2.5 h at room temperature, **2**$^+$-**BF**$_4$ was fully converted to **2-H** and **2′-H** along with the protonated base, $[^i$Pr$_2$N(H)Et$]^+[$BF$_4]^-$ (eq 4). From the ^{31}P{^{1}H} NMR spectrum, the ratio between **2-H** and **2′-H** was determined to be 3:2, which did not change with time.

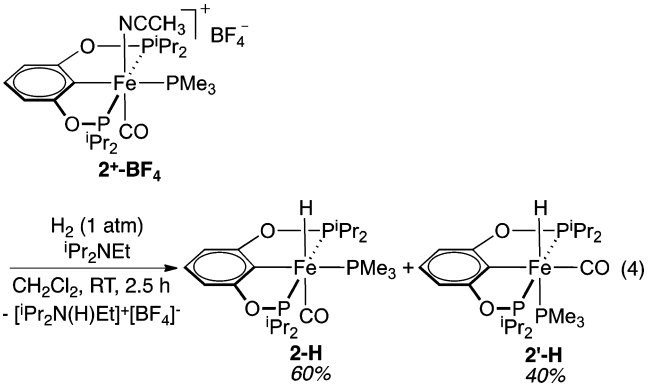

The formation of **2-H** and **2′-H** must be a kinetically controlled process, as the latter has been previously shown to be the thermodynamically more stable isomer.[15] We speculate that following the dissociation of CH_3CN from **2**$^+$-**BF**$_4$, intermediate **A** is configurationally stable enough to allow H_2 to coordinate from the site *trans* to CO (Scheme 4). The resulting dihydrogen complex **C** undergoes intermolecular deprotonation by ^{i}Pr$_2$NEt to give rise to **2-H**. Meanwhile, **C** also proceeds with *intramolecular* deprotonation by PMe_3 with concomitant migration of CO to the opposite side of the aryl group. Such a pathway involving intramolecular heterolysis of H_2 with the elimination of $[HPMe_3]^+$ may look unusual but is precedented. Tyler and co-workers have shown that *trans*-Fe(diphosphine)$_2$Cl$_2$ reacts with H_2 in water to give *trans*-$[$Fe(diphosphine)$_2$(H)(H$_2$)$]^+$Cl$^-$ along with some protonated diphosphine ligand.[36] In our case, a coordinatively unsaturated intermediate **D** is generated and reacts with free PMe_3 (available via proton transfer from $[HPMe_3]^+$ to ^{i}Pr$_2$NEt), thus explaining the formation of **2′-H**.

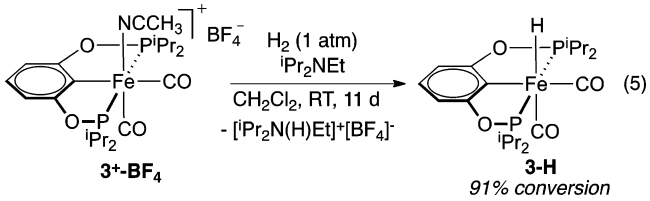

Activation of H_2 with **3**$^+$-**BF**$_4$ is significantly more sluggish (eq 5). The reaction at room temperature was incomplete even after 11 days, with 91% of **3**$^+$-**BF**$_4$ being converted to **3-H**. Presumably, the dissociation of CH_3CN from **3**$^+$-**BF**$_4$ is much slower than from **2**$^+$-**BF**$_4$. Since CF_3CO_2H failed to protonate **3-H** (Table 1), the less acidic $[^i$Pr$_2$N(H)Et$]^+[$BF$_4]^-$ is not likely to protonate **3-H** either, suggesting that the equilibrium in eq 5 lies predominantly to the right.

To activate H_2 in a catalytic fashion, hydrogenation of benzaldehyde was attempted in the presence of 1 mol % of **2**$^+$-**BF**$_4$ under ~1 atm of H_2 pressure. The limited solubility of **2**$^+$-**BF**$_4$ in commonly used organic solvents such as THF, diethyl ether, and toluene presented a minor technical challenge. Although it is highly soluble in $CHCl_3$ and CH_2Cl_2, these solvents can cause decomposition of hydride intermediates (especially if heated) and therefore are not suitable for the catalytic study. Given these factors, chlorobenzene-d_5 was chosen as the solvent so that the reaction could be conveniently monitored by NMR. Unfortunately, at 70 °C, no hydrogenation of benzaldehyde was observed at 24 h (eq 6). The ^{1}H NMR spectrum revealed a very

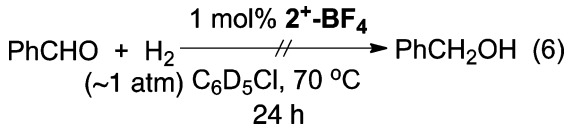

Scheme 4. Proposed Pathways Leading to the Formation of Both 2-H and 2′-H

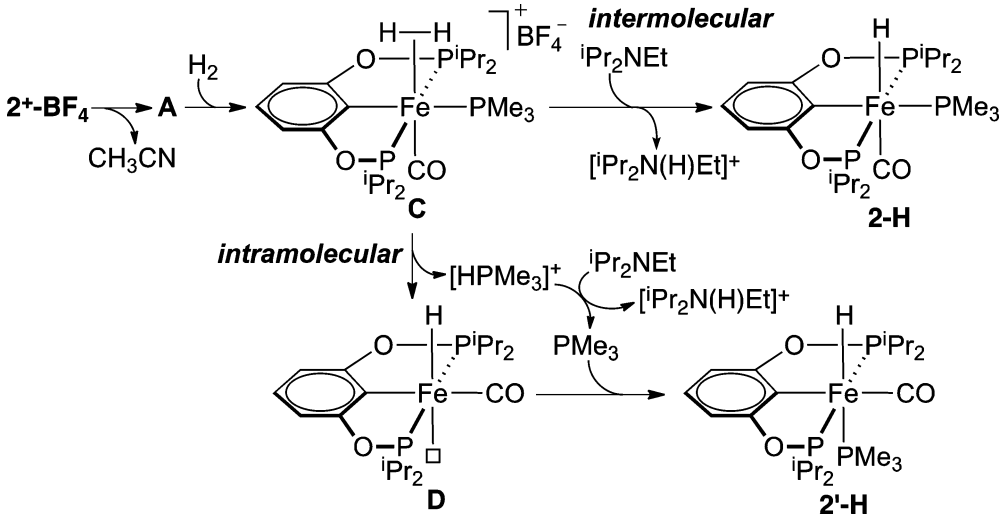

dx.doi.org/10.1021/om500758j | *Organometallics* 2014, 33, 6113−6121

small amount of hydride species at −9.47 ppm (a multiplet), and the $^{31}P\{^{1}H\}$ NMR spectrum showed substantial decomposition of the pincer complex. Because the stoichiometric activation of H_2 by **3**$^{+}$-BF_4 was much slower, catalytic hydrogenation with this particular cationic complex was not pursued.

Catalytic Hydrosilylation Reactions. Better success was achieved when the cationic complexes were employed to catalyze the hydrosilylation of carbonyl groups. As shown in Table 3, hydrosilylation of benzaldehyde (eq 7) catalyzed by

Table 3. Catalytic Hydrosilylation of Benzaldehyde[a]

entry	catalyst	time (h)	yield (%)[b]	catalyst remaining (%)[c]
1	**2**$^{+}$-BF_4	24	>99	8
2	**2-H**	24	15	95
3	**2′-H**	24	0	>99
4	**3**$^{+}$-BF_4	48	10	0
5	**3-H**	48	0	>99

[a]Conditions: iron catalyst (4.8 μmol), PhCHO (0.48 mmol), $(EtO)_3SiH$ (0.52 mmol), and hexamethylbenzene (26.5 μmol, internal standard) in 0.5 mL of C_6D_5Cl. [b]Calculated by ^{1}H NMR. [c]Calculated by $^{31}P\{^{1}H\}$ NMR.

$$\mathrm{PhCHO} + (\mathrm{EtO})_3\mathrm{SiH} \xrightarrow[\mathrm{C_6D_5Cl,\ 50\ ^oC}]{\text{1 mol\% [Fe]}} \mathrm{PhCH_2O{-}[Si]} \quad (7)$$

2^{+}-BF_4 at 50 °C went to completion in 24 h (entry 1), whereas the reaction catalyzed by the corresponding neutral iron hydride **2-H** gave hydrosilylation products[37] in 15% yield over the same period of time (entry 2). In contrast, **2′-H** did not catalyze this reaction at all (entry 3). Cationic complex **3**$^{+}$-BF_4 was not an efficient catalyst either; only 10% yield was obtained after 48 h (entry 4). However, it is still a better catalyst than **3-H**, which showed no catalytic activity (entry 5).

Overall, the cationic complexes are better catalysts than the analogous neutral hydride complexes, but only **2**$^{+}$-BF_4 shows a drastic improvement. To further understand the catalytic reactivity of these complexes, the percentage of remaining catalyst at the end of the reaction was measured by $^{31}P\{^{1}H\}$ NMR spectroscopy (the rightmost column of Table 3). In the case of **2**$^{+}$-BF_4, only 8% of the catalyst was present at the end of the reaction (entry 1). The bulk of the catalyst was converted to **2-H**, **2′-H**, and a small quantity of unidentified species. As expected from our previous study,[15] 5% of **2-H** was isomerized to **2′-H** (entry 2). For **3**$^{+}$-BF_4, the cationic species was converted to **3-H** quantitatively within 4 h, and hydrosilylated products were obtained in 10% yield (entry 4). Once **3**$^{+}$-BF_4 was fully converted to **3-H**, the catalytic reaction ceased, which is consistent with the observation of no catalytic activity for **3-H** (entry 5).

Acetophenone was also subjected to the hydrosilylation conditions using either the cationic or the neutral iron complexes as the catalysts, although the temperature had to be raised to 80 °C (eq 8). In terms of the relative catalytic

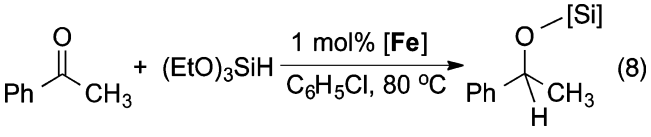

(8)

activity (Table 4), the general trend is similar to that observed in the benzaldehyde reduction. For instance, after 48 h, 79% of the acetophenone was converted to hydrosilylation products[38]

Table 4. Catalytic Hydrosilylation of Acetophenone[a]

entry	catalyst	time (h)	conversion (%)[b]
1	**2**$^{+}$-BF_4	48	79
2	**2-H**	48	54
3	**3**$^{+}$-BF_4	48	63
4	**3-H**	48	56

[a]Conditions: iron catalyst (9.5 μmol), $PhCOCH_3$ (0.95 mmol), and $(EtO)_3SiH$ (1.05 mmol) in 1 mL of C_6H_5Cl. [b]Calculated by ^{1}H NMR.

when **2**$^{+}$-BF_4 was used as the catalyst (entry 1), whereas 54% conversion was obtained for the reaction catalyzed by **2-H** (entry 2). Complex **3**$^{+}$-BF_4 (entry 3) showed a marginally better efficiency than **3-H** (entry 4), which is in agreement with the results for the hydrosilylation of benzaldehyde. It is interesting to note that for the acetophenone reaction the catalytic activity of **3-H** is comparable to that of **2-H**. For the hydrosilylation of the aldehyde mentioned above, **2-H** is a better catalyst than **3-H** (Table 3, entries 2 and 5). We hypothesize that at 80 °C the lower activity of **3-H** is offset by its higher thermal stability.

CONCLUSION

As part of our efforts to develop catalytic processes using cationic iron POCOP-pincer complexes, we have studied the protonation of four iron hydride complexes with various Brønsted acids and established the basicity order of **1-H** > **2-H** > **2′-H** > **3-H**. We have also observed a SET pathway for the reaction between **2-H** and $[Ph_3C]^{+}[BF_4]^{-}$, which results in a complicated mixture of products, making $[Ph_3C]^{+}[BF_4]^{-}$ unsuitable for the synthesis of the desired cationic complexes. Instead, we have used $HBF_4{\cdot}Et_2O$ to successfully remove the hydride ligand from **2-H**/**2′-H** and **3-H** to yield **2**$^{+}$-BF_4 and **3**$^{+}$-BF_4, respectively. Synthesis of an analogous cationic complex from **1-H** remains challenging due to the facile protonation of PMe_3. With two new cationic iron complexes in hand, we have investigated their reactivity for the activation of small molecules such as H_2 and silanes. In the presence of an external base, $^{i}Pr_2NEt$, both **2**$^{+}$-BF_4 and **3**$^{+}$-BF_4 can cleave H_2 in a heterolytic manner, resulting in neutral hydride complexes and $[^{i}Pr_2N(H)Et]^{+}[BF_4]^{-}$. Although **2**$^{+}$-$BF_4$ is not a viable catalyst for the hydrogenation of benzaldehyde (under 1 atm of H_2 pressure), **2**$^{+}$-BF_4 and **3**$^{+}$-BF_4 are effective in catalyzing the hydrosilylation of benzaldehyde and acetophenone and demonstrating improved activity over the corresponding neutral hydride complexes.

In our previous work on hydrosilylation reactions catalyzed by **1-H**,[15] deuterium-labeling experiments showed that the hydride was intact during the catalytic reaction, thus only playing the role of promoting ligand dissociation. The DFT calculations by Wei et al., however, supported a mechanism involving the delivery of the hydride to the C═O group.[17] The current cationic iron system is likely to operate via the mechanism shown in Scheme 1, which is analogous to what we have proposed for the neutral hydride system. The difference is that the silane complex in this case is cationic, resulting in more favorable silylium transfer to the carbonyl substrates. Explaining the discrepancy between the experimental data and DFT calculations for the neutral hydride catalysts would require additional investigations. Nevertheless, through this study, we have further confirmed that for the Fe-POCOP system the hydride ligand is not necessarily needed for catalytic hydrosilylation reactions.

dx.doi.org/10.1021/om500758j | Organometallics 2014, 33, 6113−6121

EXPERIMENTAL SECTION

General Comments. All the organometallic compounds were prepared and handled under an argon atmosphere using standard Schlenk and inert-atmosphere box techniques. Dry and oxygen-free solvents were collected from an Innovative Technology solvent purification system and used throughout all experiments. Deuterated NMR solvents (CD_3CN, $CDCl_3$, and C_6D_5Cl) were purchased from Cambridge Isotope Laboratories, Inc., kept under an argon atmosphere, and used without further purification. ^1H, $^{13}C\{^1H\}$, and $^{31}P\{^1H\}$ NMR spectra were recorded on a Bruker Avance-400 MHz spectrometer. Chemical shift values in ^1H and $^{13}C\{^1H\}$ NMR spectra were referenced internally to the residual solvent resonances. $^{31}P\{^1H\}$ spectra were referenced externally to 85% H_3PO_4 (0 ppm). Infrared spectra were recorded on a Thermo Scientific Nicolet 6700 FT-IR spectrometer equipped with a Smart Orbit diamond attenuated total reflectance (ATR) accessory. The mass spectrum of the reaction in eq 1 was obtained by injecting the reaction mixture (in CH_3CN) into a Micromass Q-TOF-2 mass spectrometer at a flow rate of 4 μL/min. Complexes **1-H**, **2-H**, **2′-H**, and **3-H** were prepared as described in the literature.[15]

Reaction of 2-H with $[Ph_3C]^+[BF_4]^-$. In a J. Young NMR tube, **2-H** (6.0 mg, 12 μmol) was mixed with ∼0.5 mL of CD_3CN. The hydride complex was not fully dissolved, but turned into a clear solution upon further mixing with $[Ph_3C]^+[BF_4]^-$ (3.9 mg, 12 μmol). After 1 h, the $^{31}P\{^1H\}$ NMR spectrum showed a mixture of **2-H** (45% of total pincer complexes), **2**$^+$-**BF**$_4$ (30%), **4**$^+$-**BF**$_4$ (25%), and $[HPMe_3]^+[BF_4]^-$.[39] $^{31}P\{^1H\}$ NMR (162 MHz, δ): −2.1 (s, $[HPMe_3]^+$), 0.15 (t, $^2J_{PP}$ = 17.2 Hz, PMe_3 of **2**$^+$-**BF**$_4$), 11.5 (t, $^2J_{PP}$ = 16.6 Hz, PMe_3 of **2-H**), 197.0 (s, OP^iPr_2 of **4**$^+$-**BF**$_4$), 207.3 (d, $^2J_{PP}$ = 17.2 Hz, OP^iPr_2 of **2**$^+$-**BF**$_4$), 231.9 (d, $^2J_{PP}$ = 16.6 Hz, OP^iPr_2 of **2-H**). The ^1H NMR spectrum showed **5**[40] in addition to the products mentioned above. Selected ^1H NMR data of **2-H** (400 MHz, δ): −9.41 (td, $^2J_{PH}$ = 62.8 and 50.4 Hz, Fe*H*), 0.96−1.02 (m, $CH(CH_3)_2$), 1.05−1.12 (m, $CH(CH_3)_2$), 1.41 (d, $^2J_{PH}$ = 7.2 Hz, PCH_3), 2.30−2.39 (m, $CH(CH_3)_2$), 2.43−2.55 (m, $CH(CH_3)_2$), 6.25 (d, $^3J_{HH}$ = 7.6 Hz, Ar*H*), 6.60 (t, $^3J_{HH}$ = 7.6 Hz, Ar*H*). Selected ^1H NMR data of **2**$^+$-**BF**$_4$: 1.67 (d, $^2J_{PH}$ = 8.4 Hz, PCH_3), 2.67−2.78 (m, $CH(CH_3)_2$), 6.67 (d, $^3J_{HH}$ = 8.0 Hz, Ar*H*), 7.02 (t, $^3J_{HH}$ = 8.0 Hz, Ar*H*). Selected ^1H NMR data of **4**$^+$-**BF**$_4$: 2.88−2.95 (m, $CH(CH_3)_2$), 2.96−3.05 (m, $CH(CH_3)_2$), 6.51 (d, $^3J_{HH}$ = 8.0 Hz, Ar*H*), 6.87 (t, $^3J_{HH}$ = 8.0 Hz, Ar*H*). Selected ^1H NMR data of **5**: 5.18−5.24 (m, Ph_3CCH), 5.97 (dd, $^3J_{HH}$ = 10.8 and 4.0 Hz, Ph_3CCHCH), 6.16 (dd, $^3J_{HH}$ = 10.8 Hz, $^4J_{HH}$ = 2.4 Hz, $Ph_2C{=}CCH$). ^1H NMR data of $[HPMe_3]^+[BF_4]^-$: 1.79 (dd, $^2J_{PH}$ = 15.6 Hz, $^3J_{HH}$ = 5.6 Hz, $[HP(CH_3)_3]^+$), 6.06 (dm, $^1J_{PH}$ = 508 Hz, $^3J_{HH}$ = 5.6 Hz, $[HP(CH_3)_3]^+$). TOF-MS (ES+) data of the reaction mixture (in CH_3CN, *m*/*z*): M^+ of **2**$^+$ calcd for $C_{24}H_{43}NO_3P_3Fe$ 542.1805, found 542.2819; $[M - CH_3CN]^+$ of **2**$^+$ calcd for $C_{22}H_{40}O_3P_3Fe$ 501.1540, found 501.2165; $[M - CH_3CN - CO]^+$ of **2**$^+$ calcd for $C_{21}H_{40}O_2P_3Fe$ 473.1591, found 473.2400; M^+ of **4**$^+$ calcd for $C_{23}H_{37}N_2O_3P_2Fe$ 507.1629, found 507.2582; $[M - CH_3CN]^+$ of **4**$^+$ calcd for $C_{21}H_{34}NO_3P_2Fe$ 466.1364, found 466.2246.

Procedures for the Protonation Reactions. In a J. Young NMR tube, an iron hydride complex (10 μmol) was dissolved in ∼0.5 mL of CD_3CN/THF-d_8 (1:1). The resulting solution was cooled to −30 °C, followed by the addition of $HBF_4{\cdot}Et_2O$ (10 μmol) and then slowly warmed to room temperature. For the experiments involving CF_3CO_2H or HCO_2H, the acid (10 μmol) was added at room temperature. The progress of the reaction was monitored by ^1H NMR and ^{31}P NMR spectroscopy until it reached equilibrium or for 48 h (for the reaction of **3-H** with CF_3CO_2H and the reactions of **2′-H** and **3-H** with HCO_2H). Protonation of **1-H** with CF_3CO_2H and HCO_2H was also attempted by starting the reaction at −30 °C first; however, the results were the same with a significant amount of decomposition products observed.

Synthesis of {[2,6-(^{i}Pr$_2$PO)$_2$C$_6$H$_3$]Fe(CO)(PMe$_3$)(CH$_3$CN)}$^+$-[BF$_4$]$^-$ (2$^+$-BF$_4$). A solution of **2-H** (100 mg, 0.20 mmol) in THF/CH_3CN (1 mL each) was cooled to −30 °C, followed by the addition of $HBF_4{\cdot}Et_2O$ (28 μL, 0.20 mmol) at this temperature. The reaction mixture was then slowly warmed to room temperature while gas evolution was observed. The resulting bright yellow solution was passed through a short pad of Celite, and the solvent was removed under vacuum to produce a crystalline solid (107 mg, 85% yield). ^1H NMR (400 MHz, $CDCl_3$, δ): 1.29−1.41 (m, $CH(CH_3)_2$, 24H), 1.73 (d, $^2J_{PH}$ = 8.4 Hz, PMe_3, 9H), 2.38 (s, $NCCH_3$, 3H), 2.68−2.79 (m, C*H*, 4H), 6.66 (d, $^3J_{HH}$ = 8.0 Hz, Ar*H*, 2H), 6.99 (t, $^3J_{HH}$ = 8.0 Hz, Ar*H*, 1H). $^{13}C\{^1H\}$ NMR (101 MHz, $CDCl_3$, δ): 4.9 (s, CH_3CN), 18.0 (s, CH_3), 18.1 (s, CH_3), 18.5 (s, CH_3), 18.6 (s, CH_3), 21.1 (d, $^1J_{PC}$ = 26.4 Hz, PMe_3), 31.3 (t, $^1J_{PC}$ = 7.2 Hz, CH), 32.2 (t, $^1J_{PC}$ = 10.4 Hz, CH), 106.7 (t, $^3J_{PC}$ = 4.7 Hz, ArC), 128.1 (s, ArC), 132.9 (s, CH_3CN), 134.4−135.0 (m, ArC), 164.0 (t, $^2J_{PC}$ = 6.5 Hz, ArC), 216.3-216.5 (m, CO). $^{31}P\{^1H\}$ NMR (162 MHz, $CDCl_3$, δ): −0.2 (t, $^2J_{PP}$ = 16.5 Hz, PMe_3, 1P), 206.4 (d, $^2J_{PP}$ = 16.5 Hz, OP^iPr_2, 2P). ATR-IR (solid): ν_{CO} = 1946 cm^{-1}. Anal. Calcd for $C_{24}H_{43}NO_3P_3FeBF_4$: C, 45.82; H, 6.89; N, 2.23. Found: C, 45.83; H, 6.85; N, 2.38.

Synthesis of *cis*-{[2,6-(^{i}Pr$_2$PO)$_2$C$_6$H$_3$]Fe(CO)$_2$(CH$_3$CN)}$^+$[BF$_4$]$^-$ (3$^+$-BF$_4$). This compound was prepared in 82% yield by a procedure similar to that used for **2**$^+$-**BF**$_4$. ^1H NMR (400 MHz, $CDCl_3$, δ): 1.30−1.54 (m, $CH(CH_3)_2$, 24H), 2.42 (s, $NCCH_3$, 3H), 2.74−2.84 (m, C*H*, 2H), 2.89−2.98 (m, C*H*, 2H), 6.75 (d, $^2J_{HH}$ = 8.0 Hz, Ar*H*, 2H), 7.10 (t, $^2J_{HH}$ = 8.0 Hz, Ar*H*, 1H). $^{13}C\{^1H\}$ NMR (101 MHz, $CDCl_3$, δ): 4.7 (s, CH_3CN), 16.7 (s, CH_3), 17.1 (t, $^2J_{PC}$ = 2.0 Hz, CH_3), 17.3 (s, CH_3), 18.6 (t, $^2J_{PC}$ = 2.4 Hz, CH_3), 29.2 (t, $^1J_{PC}$ = 12.9 Hz, CH), 30.7 (t, $^1J_{PC}$ = 10.6 Hz, CH), 108.1 (t, $^3J_{PC}$ = 5.5 Hz, ArC), 129.8 (s, ArC), 131.9 (t, $^2J_{PC}$ = 12.6 Hz, ArC), 132.8 (s, CH_3CN), 164.5 (t, $^2J_{PC}$ = 7.1 Hz, ArC), 205.5 (t, $^2J_{PC}$ = 8.3 Hz, CO), 210.5 (t, $^2J_{PC}$ = 27.2 Hz, CO). $^{31}P\{^1H\}$ NMR (162 MHz, $CDCl_3$, δ): 206.9 (s). ATR-IR (solid): ν_{CO} = 2046 and 1989 cm^{-1}. Anal. Calcd for $C_{22}H_{34}NO_4P_2FeBF_4$: C, 45.47; H, 5.90; N, 2.41. Found: C, 45.41; H, 5.75; N, 2.56.

X-ray Structure Determination. Single crystals of **2**$^+$-**BF**$_4$ were grown from a saturated solution in THF/CH_3CN (or CH_2Cl_2) at −30 °C. Crystal data collection and refinement parameters are summarized in Table S1. Intensity data were collected at 150 K on a Bruker APEX-II CCD detector at Beamline 11.3.1 at the Advanced Light Source (Lawrence Berkeley National Laboratory) using synchrotron radiation tuned to λ = 0.774 90 Å. The data frames were collected using the program APEX2 and processed using the program SAINT, a routine within APEX2. The data were corrected for absorption and beam corrections based on the multiscan technique as implemented in SADABS. The structure was solved by a combination of direct methods SHELXTL v6.14 and the difference Fourier technique and refined by full-matrix least-squares on F^2. Non-hydrogen atoms were refined with anisotropic displacement parameters. The BF_4^- anion is disordered; a reasonable two-component disorder model is given (major occupancy = 0.67). The H atom positions were calculated and treated with a riding model in subsequent refinements. The isotropic displacement parameters for the H atoms were defined as aU_{eq} (*a* = 1.5 for methyl and 1.2 for all others) of the adjacent atom.

Attempted Hydrogenation of Benzaldehyde. In a J. Young NMR tube, **2**$^+$-**BF**$_4$ (3.0 mg, 4.8 μmol) was mixed with 0.5 mL of C_6D_5Cl, followed by the addition of benzaldehyde (49 μL, 0.48 mmol) and hexamethylbenzene (4.3 mg, 26.5 μmol, internal standard). The reaction mixture was frozen by liquid nitrogen, after which the headspace of the NMR tube was evacuated and then exposed to a hydrogen atmosphere (1 atm). The frozen sample was thawed at room temperature before the NMR tube was disconnected from the hydrogen source. The reaction mixture was heated by an oil bath at 70 °C, and the progress of the reaction was monitored by ^1H and $^{31}P\{^1H\}$ NMR spectroscopy.

General Procedure for Catalytic Hydrosilylation of Benzaldehyde. In a typical experiment, an iron catalyst (4.8 μmol, 1 mol %) and 0.5 mL of C_6D_5Cl were mixed in a J. Young NMR tube. To this solution, benzaldehyde (49 μL, 0.48 mmol), triethoxysilane (96 μL, 0.52 mmol), and hexamethylbenzene (4.3 mg, 26.5 μmol, internal standard) were added at once. The reaction mixture was heated by an oil bath at 50 °C, and the progress of the reaction was monitored by ^1H and $^{31}P\{^1H\}$ NMR spectroscopy. The combined yield for the

dx.doi.org/10.1021/om500758j | Organometallics 2014, 33, 6113−6121

hydrosilylation products was calculated by comparing the integration of $PhCH_2O$ methylene resonances[15] with that of the internal standard. The percentage of the remaining iron catalyst was calculated from ^{31}P NMR integrations of the iron catalysts and other iron species (without a standard).

General Procedure for Catalytic Hydrosilylation of Acetophenone. In a typical experiment, an iron catalyst (9.5 μmol, 1 mol %) was dissolved in 1 mL of C_6H_5Cl. To this solution, acetophenone (111 μL, 0.95 mmol) and triethoxysilane (194 μL, 1.05 mmol) were added. The reaction mixture was heated by an oil bath at 80 °C for 48 h. After cooling to room temperature, an aliquot was withdrawn from the mixture, diluted with $CDCl_3$, and then subjected to ^1H NMR analysis. No byproducts were observed for any of the reactions with acetophenone. The percentage conversion of acetophenone was calculated based on the integrations of $PhCH(OSiR_3)CH_3$ and $PhCOCH_3$.[15]

■ ASSOCIATED CONTENT

Supporting Information

Complete details of the crystallographic study (PDF and CIF), characterization data for 2^+-BF_4 and 3^+-BF_4, and representative NMR spectra of the catalytic reaction. This material is available free of charge via the Internet at http://pubs.acs.org.

■ AUTHOR INFORMATION

Corresponding Author

*E-mail: hairong.guan@uc.edu.

Notes

The authors declare no competing financial interest.

■ ACKNOWLEDGMENTS

We thank the National Science Foundation (CHE-0952083) and the Alfred P. Sloan Foundation (research fellowship to H.G.) for supporting this research. Crystallographic data were collected at Beamline 11.3.1 at the Advanced Light Source (ALS), Lawrence Berkeley National Laboratory (supported by the U.S. Department of Energy, Office of Basic Energy Sciences, under contract No. DE-AC02-05CH11231).

■ REFERENCES

(1) (a) *The Handbook of Homogeneous Hydrogenation*; de Vries, J. G., Elsevier, C. J., Eds.; Wiley-VCH: Weinheim, Germany, 2007. (b) *Modern Reduction Methods*; Andersson, P. G., Munslow, I. J., Eds.; Wiley-VCH: Weinheim, Germany, 2008.

(2) For reviews on activation of H_2, see: (a) Kubas, G. J. *Chem. Rev.* **2007**, *107*, 4152−4205. (b) Szymczak, N. K.; Tyler, D. R. *Coord. Chem. Rev.* **2008**, *252*, 212−230. (c) Morris, R. H. *Coord. Chem. Rev.* **2008**, *252*, 2381−2394. (d) Kubas, G. J. *J. Organomet. Chem.* **2009**, *694*, 2648−2653. (e) Eisenstein, O.; Crabtree, R. H. *New J. Chem.* **2013**, *37*, 21−27. (f) Kubas, G. J. *J. Organomet. Chem.* **2014**, *715*, 33−49.

(3) For reviews on activation of silanes and boranes, see: (a) Corey, J. Y.; Braddock-Wilking, J. *Chem. Rev.* **1999**, *99*, 175−292. (b) Lin, Z. *Chem. Soc. Rev.* **2002**, *31*, 239−245. (c) Nikonov, G. I. *Adv. Organomet. Chem.* **2005**, *53*, 217−309. (d) Corey, J. Y. *Chem. Rev.* **2011**, *111*, 863−1071. (e) Perutz, R. N.; Sabo-Etienne, S. *Angew. Chem., Int. Ed.* **2007**, *46*, 2578−2592. (f) Alcaraz, G.; Grellier, M.; Sabo-Etienne, S. *Acc. Chem. Res.* **2009**, *42*, 1640−1649. (g) Pandey, K. K. *Coord. Chem. Rev.* **2009**, *253*, 37−55.

(4) Chakraborty, S.; Guan, H. *Dalton Trans.* **2010**, *39*, 7427−7436.

(5) For representative examples, see: (a) Fagan, P. J.; Voges, M. H.; Bullock, R. M. *Organometallics* **2010**, *29*, 1045−1048. (b) Dobereiner, G. E.; Nova, A.; Schley, N. D.; Hazari, N.; Miller, S. J.; Eisenstein, O.; Crabtree, R. H. *J. Am. Chem. Soc.* **2011**, *133*, 7547−7562.

(6) Mo- and W-based catalysts: (a) Dioumaev, V. K.; Bullock, R. M. *Nature* **2000**, *424*, 530−532. (b) Chakraborty, S.; Blacque, O.; Fox, T.; Berke, H. *ACS Catal.* **2013**, *3*, 2208−2217.

(7) Re-based catalysts: (a) Ison, E. A.; Trivedi, E. R.; Corbin, R. A.; Abu-Omar, M. M. *J. Am. Chem. Soc.* **2005**, *127*, 15374−15375. (b) Du, G.; Abu-Omar, M. M. *Organometallics* **2006**, *25*, 4920−4923. (c) Gu, P.; Wang, W.; Wang, Y.; Wei, H. *Organometallics* **2013**, *32*, 47−51.

(8) Fe-based catalysts: (a) Gutsulyak, D. V.; Kuzmina, L. G.; Howard, J. A. K.; Vyboishchikov, S. F.; Nikonov, G. I. *J. Am. Chem. Soc.* **2008**, *130*, 3732−3733. (b) Bézier, D.; Jiang, F.; Roisnel, T.; Sortais, J.-B.; Darcel, C. *Eur. J. Inorg. Chem.* **2012**, 1333−1337. (c) Bézier, D.; Venkanna, G. T.; Misal Castro, L. C.; Zheng, J.; Roisnel, T.; Sortais, J.-B.; Darcel, C. *Adv. Synth. Catal.* **2012**, *354*, 1879−1884. (d) Zheng, J.; Misal Castro, L. C.; Roisnel, T.; Darcel, C.; Sortais, J.-B. *Inorg. Chim. Acta* **2012**, *380*, 301−307. (e) César, V.; Misal Castro, L. C.; Dombray, T.; Sortais, J.-B.; Darcel, C.; Labat, S.; Miqueu, K.; Sotiropoulos, J.-M.; Brousses, R.; Lugan, N.; Lavigne, G. *Organometallics* **2013**, *32*, 4643−4655. (f) Kumar, D.; Prakasham, A. P.; Bheeter, L. P.; Sortais, J.-B.; Gangwar, M.; Roisnel, T.; Kalita, A. C.; Darcel, C.; Ghosh, P. *J. Organomet. Chem.* **2014**, *762*, 81−87.

(9) Ru-based catalysts: (a) Gutsulyak, D. V.; Vyboishchikov, S. F.; Nikonov, G. I. *J. Am. Chem. Soc.* **2010**, *132*, 5950−5951. (b) Gutsulyak, D. V.; Nikonov, G. I. *Angew. Chem., Int. Ed.* **2010**, *49*, 7553−7556. (c) Gutsulyak, D. V.; van der Est, A.; Nikonov, G. I. *Angew. Chem., Int. Ed.* **2011**, *50*, 1384−1387. (d) Gutsulyak, D. V.; Nikonov, G. I. *Adv. Synth. Catal.* **2012**, *354*, 607−611. (e) Lee, S.-H.; Gutsulyak, D. V.; Nikonov, G. I. *Organometallics* **2013**, *32*, 4457−4464. (f) Lee, S.-H.; Nikonov, G. I. *Dalton Trans.* **2014**, *43*, 8888−8893. (g) Abbina, S.; Bian, S.; Oian, C.; Du, G. *ACS Catal.* **2013**, *3*, 678−684.

(10) Ir-based catalysts: (a) Yang, J.; Brookhart, M. *J. Am. Chem. Soc.* **2007**, *129*, 12656−12657. (b) Yang, J.; White, P. S.; Brookhart, M. *J. Am. Chem. Soc.* **2008**, *130*, 17509−17518. (c) Yang, J.; Brookhart, M. *Adv. Synth. Catal.* **2009**, *351*, 175−187. (d) Park, S.; Brookhart, M. *Organometallics* **2010**, *29*, 6057−6064. (e) Park, S.; Brookhart, M. *Chem. Commun.* **2011**, *47*, 3643−3645. (f) Park, S.; Brookhart, M. *J. Am. Chem. Soc.* **2012**, *134*, 640−653. (g) Park, S.; Bézier, D.; Brookhart, M. *J. Am. Chem. Soc.* **2012**, *134*, 11404−11407. (h) McLaughlin, M. P.; Adduci, L. L.; Becker, J. J.; Gagné, M. R. *J. Am. Chem. Soc.* **2013**, *135*, 1225−1227.

(11) Ni-based catalysts: Bheeter, L. P.; Henrion, M.; Chetcuti, M. J.; Darcel, C.; Ritleng, V.; Sortais, J.-B. *Catal. Sci. Technol.* **2013**, *3*, 3111−3116.

(12) (a) Bullock, R. M. *Chem.—Eur. J.* **2004**, *10*, 2366−2374. (b) Bullock. R. M. Ionic Hydrogenations. In *The Handbook of Homogeneous Hydrogenation*; de Vries, J. G., Elsevier, C. J., Eds.; Wiley-VCH: Weinheim, Germany, 2007; pp 153−197.

(13) Et_3SiH was shown to coordinate to the cationic iridium center in an η^1-fashion. For details, see: Yang, J.; White, P. S.; Schauer, C. K.; Brookhart, M. *Angew. Chem., Int. Ed.* **2008**, *47*, 4141−4143.

(14) A very recent mechanistic study has shown that the most active hydride intermediate is not the hydride species produced after silylium transfer, but a silane-bound iridium hydride. For details, see: Metsänen, T. T.; Hrobárik, P.; Klare, H. F. T.; Kaupp, M.; Oestreich, M. *J. Am. Chem. Soc.* **2014**, *136*, 6912−6915.

(15) Bhattacharya, P.; Krause, J. A.; Guan, H. *Organometallics* **2011**, *30*, 4720−4729.

(16) Bhattacharya, P.; Krause, J. A.; Guan, H. *J. Am. Chem. Soc.* **2014**, *136*, 11153−11161.

(17) Wang, W.; Gu, P.; Wang, Y.; Wei, H. *Organometallics* **2014**, *33*, 847−857.

(18) (a) Zhang, J.; Medley, C. M.; Krause, J. A.; Guan, H. *Organometallics* **2010**, *29*, 6393−6401. (b) Hao, J.; Mougang-Soumé, B.; Vabre, B.; Zargarian, D. *Angew. Chem., Int. Ed.* **2014**, *53*, 3218−3222.

(19) McBride, J. M. *Tetrahedron* **1974**, *30*, 2009−2022.

(20) (a) Ryan, O. B.; Tilset, M.; Parker, V. D. *J. Am. Chem. Soc.* **1990**, *112*, 2618−2626. (b) Guan, H.; Saddoughi, S. A.; Shaw, A. P.; Norton, J. R. *Organometallics* **2005**, *24*, 6358−6364.

(21) (a) Besora, M.; Lledós, A.; Maseras, F. *Chem. Soc. Rev.* **2009**, *38*, 957−966. (b) Belkova, N. V.; Epstein, L. M.; Shubina, E. S. *Eur. J. Inorg. Chem.* **2010**, 3555−3565.
(22) Izutsu, K. *Acid Base Dissociation Constants in Dipolar Aprotic Solvents*; Blackwell Scientific: Oxford, U.K., 1990; IUPAC Chemical Data Series No. 35.
(23) The pK_a value in THF should be different. For the conversion of pK_a values between CH_3CN and THF, see: (a) Abdur-Rashid, K.; Fong, T. P.; Greaves, B.; Gusev, D. G.; Hinman, J. G.; Landau, S. E.; Lough, A. J.; Morris, R. H. *J. Am. Chem. Soc.* **2000**, *122*, 9155−9171. (b) Morris, R. H. *J. Am. Chem. Soc.* **2014**, *136*, 1948−1959.
(24) The pK_a values for HCO_2H and CF_3CO_2H in water are 3.75 and 0.52, respectively. These numbers were obtained from the following book: Anslyn, E. V.; Dougherty, D. A. *Modern Physical Organic Chemistry*; University Science Books: Sausalito, CA, 2006; p 279.
(25) (a) Papish, E. T.; Rix, F. C.; Spetseris, N.; Norton, J. R. *J. Am. Chem. Soc.* **2000**, *122*, 12235−12242. (b) Henry, R. M.; Shoemaker, R. K.; DuBois, D. L.; DuBois, M. R. *J. Am. Chem. Soc.* **2006**, *128*, 3002−3010. (c) Baya, M.; Maresca, O.; Poli, R.; Coppel, Y.; Maseras, F.; Lledós, A.; Belkova, N. V.; Dub, P. A.; Epstein, L. M.; Shubina, E. S. *Inorg. Chem.* **2006**, *45*, 10248−10262.
(26) Roddick, D. M. *Top. Organomet. Chem.* **2013**, *40*, 49−88.
(27) The pincer backbone of related six-coordinate ruthenium POCOP-pincer complexes appears to be as flat as that in most other POCOP-pincer complexes. For structures of ruthenium POCOP-pincer complexes, see: Bedford, R. B.; Betham, M.; Blake, M. E.; Coles, S. J.; Draper, S. M.; Hursthouse, M. B.; Scully, P. N. *Inorg. Chim. Acta* **2006**, *359*, 1870−1878.
(28) The deviation from planarity for the C1−O1−O2−Fe plane was calculated to be 0.0238 Å. The deviation signs are arbitrary; opposite signs for P1 and P2 mean that they are on opposite sides of the least-squares plane.
(29) The deviation from planarity for the C1−O1−O2−Fe plane was calculated to be 0.0042 Å.
(30) (a) Benito-Garagorri, D.; Becker, E.; Wiedermann, J.; Lackner, W.; Pollak, M.; Mereiter, K.; Kisala, J.; Kirchner, K. *Organometallics* **2006**, *25*, 1900−1913. (b) Benito-Garagorri, D.; Kirchner, K. *Acc. Chem. Res.* **2008**, *41*, 201−213.
(31) (a) Benito-Garagorri, D.; Alves, L. G.; Veiros, L. F.; Standfest-Hauser, C. M.; Tanaka, S.; Mereiter, K.; Kirchner, K. *Organometallics* **2010**, *29*, 4932−4942. (b) Benito-Garagorri, D.; Lagoja, I.; Veiros, L. F.; Kirchner, K. A. *Dalton Trans.* **2011**, *40*, 4778−4792.
(32) Rybtchinski, B.; Ben-David, Y.; Milstein, D. *Organometallics* **1997**, *16*, 3786−3793.
(33) (a) Benito-Garagorri, D.; Puchberger, M.; Mereiter, K.; Kirchner, K. *Angew. Chem., Int. Ed.* **2008**, *47*, 9142−9145. (b) Benito-Garagorri, D.; Alves, L. G.; Puchberger, M.; Mereiter, K.; Veiros, L. F.; Calhorda, M. J.; Carvalho, M. D.; Ferreira, L. P.; Godinho, M.; Kirchner, K. *Organometallics* **2009**, *28*, 6902−6914.
(34) Li, S.; Hall, M. B. *Organometallics* **1999**, *18*, 5682−5687.
(35) (a) Rachidi, I. E.-I.; Eisenstein, O.; Jean, Y. *New J. Chem.* **1990**, *14*, 671−677. (b) Riehl, J.-F.; Jean, Y.; Eisenstein, O.; Pélissier, M. *Organometallics* **1992**, *11*, 729−737.
(36) (a) Gilbertson, J. D.; Szymczak, N. K.; Tyler, D. R. *Inorg. Chem.* **2004**, *43*, 3341−3343. (b) Gilbertson, J. D.; Szymczak, N. K.; Crossland, J. L.; Miller, W. K.; Lyon, D. K.; Foxman, B. M.; Davis, J.; Tyler, D. R. *Inorg. Chem.* **2007**, *46*, 1205−1214.
(37) Multiple hydrosilylation products were observed for the reactions described in Table 3 (entries 1, 2, and 4). This is due to the redistribution of $PhCH_2O$ and EtO groups on silicon.
(38) There were two hydrosilylation products, as evidenced by two methine resonances (overlapped in the region of 5.1−5.2 ppm).
(39) Bellachioma, G.; Cardaci, G.; Macchioni, A.; Venturi, C.; Zuccaccia, C. *J. Organomet. Chem.* **2006**, *691*, 3881−3888.
(40) Chen, C.; Lee, H.; Jordan, R. F. *Organometallics* **2010**, *29*, 5373−5381.